Space charges and dipoles in rare-earth-doped SrF_2

P. Dorenbos and H. W. den Hartog
Solid State Physics Laboratory, University of Groningen, 1 Melkweg, 9718 EP Groningen, The Netherlands
(Received 9 October 1984)

The high-temperature peak, observed with ionic thermocurrent (ITC) experiments performed on RF_3-doped SrF_2, CaF_2, and BaF_2, is proved to be related to space charges. Measurements of R^{3+}-F^- dipole concentrations as a function of RF_3 doping concentration in SrF_2 are presented (R=La, Ce, Nd, Eu, Sm, Gd, Dy, Er, Yb, and Lu). The results as a function of RF_3 doping concentration can be explained by assuming that only isolated R^{3+}-F^- dipoles are observed with ITC. The results as a function of R^{3+} ionic radius can be explained by assuming an increasing clustering probability of the R^{3+} ions as the radius of the rare-earth ions decreases. It is concluded that the large rare-earth ions are distributed randomly over the SrF_2 lattice, while the small R^{3+} ions tend to cluster during crystal growth.

I. INTRODUCTION

Much experimental work has been performed to elucidate the defect structure and phenomena related with ionic motion in RF_3-doped MF_2 single crystals[1–16] (R^{3+}=rare-earth ion; M=Sr, Ca, or Ba). Doping MF_2 with RF_3 leads to substitution of a M^{2+} ion by a R^{3+} ion. An extra F^-, necessary for charge compensation, occupies an interstitial position. Depending upon the location of this F^-, with respect to a rare-earth ion, three positions are distinguished: (i) F^- at a nearest-neighbor (NN) interstitial position of a R^{3+} (NN dipolar complex)—this R^{3+} has a tetragonally symmetric environment; (ii) F^- at a next-nearest-neighbor (NNN) position (NNN) dipolar complex)—this R^{3+} site is characterized by trigonal symmetry; (iii) nonlocal charge compensation, F^- is not at a NN or NNN position and is called a free interstitial F^- ion—this R^{3+} site is characterized by cubic symmetry.

Static properties concerning defect structures (site symmetries of R^{3+}) have been studied with ESR, electron-nuclear double resonance, and the electric field effect in ESR; dynamic properties (reorientation kinetics of dipoles, ionic conductivity) have been studied with ionic thermocurrent (ITC) and dielectric loss experiments. It is now well established that at low RF_3 concentrations NN dipoles are the predominant dipolar defects in CaF_2,[1–4] while in BaF_2, NNN dipoles are predominant.[4,6,7] In SrF_2 both dipoles are observed. If R=La, Ce, Pr, Nd, Sm, or Eu, NN dipoles are dominant. NNN dipoles are the dominant ones if R=Tb, Dy, Er, Tm, Yb, or Lu.[4,5] These experimental observations have also been confirmed by theoretical calculations.[17,18]

A very intense relaxation peak, observed with ITC experiments at high temperatures (300–400 K), has often been associated with space charge relaxation of free interstitial F^- ions.[8–10] The position of this peak strongly depends on rare-earth concentration, while the intensity is concentration independent. Within the last few years a systematic study has been performed on the interpretation of this peak where attention was focused at the position and the width of this peak.[10–16]

In this paper we will concentrate on the intensity of the relaxation peaks observed in ITC spectra of SrF_2 doped with RF_3 as a function of RF_3 concentration and as a function of rare-earth ionic radius. We will show that the intensity of the high-temperature (HT) peak can be explained by assuming that space charges are responsible for this peak. This can be done by using a theory developed by Müller.[19] The concentration of dipoles, observed with ITC experiments, as a function of R^{3+} concentration can be explained by assuming that only isolated dipoles contribute to the NN or NNN dipole relaxation peak. The number of isolated dipoles is determined by a random distribution of R^{3+} ions over the fluorite lattice if large R^{3+} are involved. If small R^{3+} ions are involved, clustering of R^{3+} during crystal growth is also important.

II. EXPERIMENTAL PROCEDURES

The experimental setup and procedures for the growth of the single-crystal materials have been described elsewhere.[5,12] For the ITC experiments cylindrical samples were used (diameter 7–8 mm and thickness 1–2 mm). An insulating material was inserted between sample surfaces and electrodes (Teflon or Mylar foils). The polarization temperature was chosen well above the position of the high-temperature peak and a polarizing voltage of 4 kV was used. The polarization time was always 5 min. During the depolarization phase the temperature is increased linearly with time (0.05 K/s). The concentrations of trivalent impurities have been determined with the x-ray fluorescence method. Below 1 mol%, this method does not work because the sensitivity is too low. Therefore, we have employed here the nominal concentration.

III. THEORY

During polarization of a crystal, two processes may take place: (i) polarization of bound charges like NN and NNN dipoles; (ii) polarization of free charges leading to the accumulation of space charges at the sample surfaces. The strength of the polarization depends on the sample cell configuration. In the case of blocking electrodes (e.g., painted silver electrodes) the accumulation of space

charges is stopped when the drift current due to the applied polarization field equals the diffusion current due to the concentration gradient at the sample surface. This situation has been described by MacDonald.[20,21] In the case of insulating electrodes (Teflon foils between sample and electrodes), the accumulation of space charges is stopped when the electric field in the bulk of the crystal becomes zero. Most of the polarizing field is then across the insulating foils. This situation has been described by Müller[19] and is applicable to our experimental situation. A short outline of this theory will be given below.

If free and mobile charge carriers are present, the crystal can be considered as a conducting medium. The situation is drawn in Fig. 1(a). Charging of the capacitances between electrodes and sample surfaces will take place during polarization. The accumulated charge Q is, if in equilibrium, equal to $C_I U_p$. C_I is the series capacitance of the capacitances between sample surfaces and upper and lower electrodes. U_p is the polarizing voltage. Because now there is no electric field inside the crystal, polarization of dipoles does not occur. Short-circuiting the electrodes at liquid-nitrogen temperature via an electrometer gives the situation presented in Fig. 1(b). Because the free-charge carries have a very low mobility at this temperature, the sample acts as an insulating medium with a capacitance C_s and a new equilibrium situation is obtained. It is easy to show that the relation between the electrode charge Q_e and the frozen in space charge Q is[19]

$$Q_e = Q\frac{C_I}{C_I + C_s} . \tag{1}$$

The electric field inside the crystal due to the space charge Q is given by

$$E_s = \frac{Q}{d_s}\frac{1}{C_s + C_I} , \tag{2}$$

where d_s is the thickness of the sample.

During subsequent heating of the crystal, well before relaxation of the space charges, polarization of dipoles due to the field E_s occurs. The polarization P is given by Langevin's equation:

$$P = \frac{N_d \mu^2}{3k_B T} E_s , \tag{3}$$

where N_d is the dipole concentration (m^{-3}), μ is the dipole moment (C m), k_B is Boltzmann's constant, and T the temperature (K). Due to the dipole polarization, the capacitance C_s increases by

$$C_d = \frac{N_d \mu^2 A}{3k_B T d_s} , \tag{4}$$

where A is the area of the sample surface. The change in electrode charge, due to the dipole polarization, leads to the dipole polarization peak observed in ITC spectra. The charge Q_d contained in this peak is, using Eqs. (1) and (4), given by

$$Q_d = \frac{Q C_I C_d}{(C_I + C_s)(C_I + C_s + C_d)} . \tag{5}$$

The charge Q_{SC} contained in the space-charge relaxation peak is the charge left on the electrodes and can be given by

$$Q_{SC} = \frac{C_I^2 U_p}{C_I + C_s + \sum_d C_d} . \tag{6}$$

$\sum_d C_I$ is the summation over all the dipole contributions to the sample capacitance.

If a linear heating scheme is used during the ITC experiment and the conductivity of the sample can be described by

$$\sigma(T) = \sigma_0 \exp\left[\frac{-E}{k_B T}\right] , \tag{7}$$

the condition for the maximum of the space-charge-relaxation peak is given by[19]

$$\frac{k_B T_m^2}{b(C_I + C_s)E}\frac{A}{d_s}\sigma(T) = 1 , \tag{8}$$

where T_m is the position of the maximum of the space-charge relaxation peak and b the heating rate during the ITC experiment. Equation (8) can be approximated by

$$T_m = T_0 + \ln\left[\frac{C_I + C_s}{C_s}\right]\left[\frac{2}{T_0} + \frac{E}{k_B T_0^2}\right]^{-1} , \tag{9}$$

where T_0 is the position of the space-charge peak if C_s goes to infinity. The position of the space-charge relaxation peak is, therefore, dependent on C_I and C_s. It can also be shown that the width of the space-charge peak is slightly dependent on C_I and C_s and that the positions of dipole relaxation peaks are independent on C_I and C_s.

By varying the thickness of insulating material and sample, it is now possible to discriminate between dipole relaxation peaks and space-charge relaxation peaks. Furthermore, if μ is known, the number of dipoles N_d can be calculated.

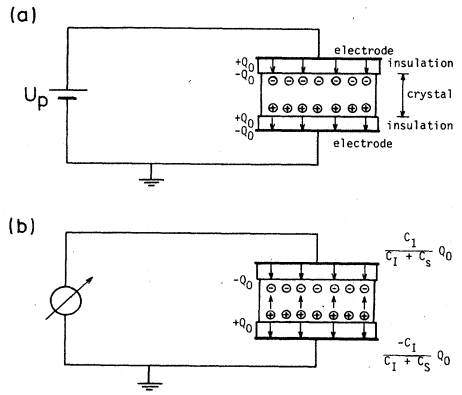

FIG. 1. (a) Experimental situation in our ITC setup after polarizing a conducting sample isolated by Teflon or Mylar foils from the electrodes. (b) Situation obtained at liquid-nitrogen temperature if the electrodes are short-circuited and a frozen-in charge Q_0 at the sample surface is present.

IV. EXPERIMENTAL RESULTS

A. HT peak

We have performed ITC measurements with sample thicknesses between 0.3 and 4.5 mm and Mylar insulation thicknesses between 0.023 and 0.175 mm. We used a SrF_2 single crystal, doped with 0.334 mol% GdF_3, as testing material.

In Fig. 2 ITC spectra as a function of sample thickness are shown. The thickness of insulation material was kept constant (0.1-mm Teflon foils). A drastic decrease of the HT-peak intensity is observed as d_s decreases. There is also a shift in HT-peak position toward higher temperatures as the sample thickness is increased, while the dipole relaxation peaks are located at fixed positions.

Usually $C_d \ll C_I + C_s$; defining $a = C_I/C_s$, Eqs. (5) and (6) can be approximated by

$$Q_{SC} = C_I U_p \left[\frac{a}{1+a}\right], \tag{10a}$$

$$Q_d d_s = C_d d_s U_p \left[\frac{1}{1+a}\right]^2. \tag{10b}$$

In Fig. 3(a) we have plotted $Q_{SC}/C_I U_p$ as a function of a. In Fig. 3(b), $Q_{NN} d_s$ as a function of a is shown. We also show the theoretical curves expressed by Eq. (10) where we have used a least-squares fit value for C_d. The rather large error bars are due to difficulties in measuring the capacitance of the thin insulating layers and we did not take into account fringing field effects in capacitance C_s either. In addition we verified the linear relationship between the peak intensities and the polarizing voltage U_p.

The correspondence between Eqs. (10) and the experimental peak intensities is evident. Also taking into account the shift of the HT peak as a function of sample thickness, as shown in Fig. 2 and expressed by Eq. (9), we arrive at the following conclusion: The high-temperature peak, observed in ITC experiments performed on rare-earth-doped SrF_2, CaF_2, and BaF_2 is associated with space-charge relaxation of free-charge carriers.

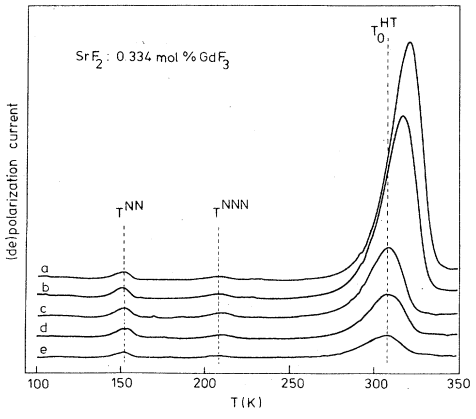

FIG. 2. ITC spectra obtained for 0.334 mol% GdF_3 doped in SrF_2 crystals as a function of sample thickness (d_s). Teflon foils with a thickness of 0.1 mm were used as insulating material. (a) $d_s = 4.4$ mm; (b) $d_s = 2.5$ mm; (c) $d_s = 1.0$ mm; (d) $d_s = 0.6$ mm; (e) $d_s = 0.3$ mm.

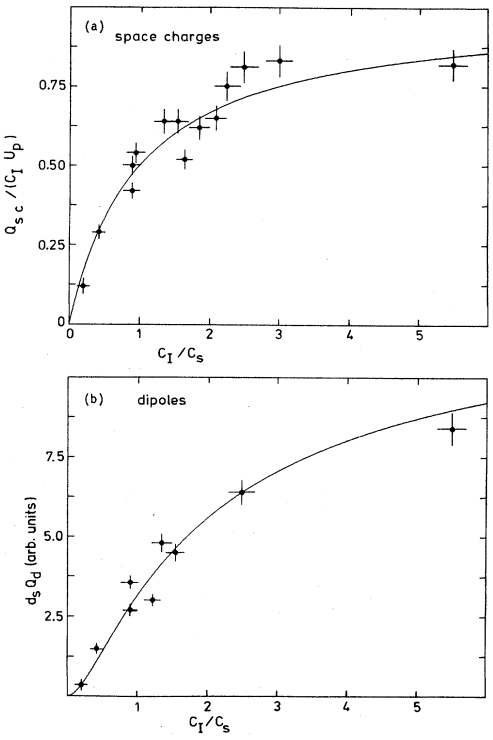

FIG. 3. (a) $Q_{SC}/C_I U_p$ as a function of C_I/C_s obtained for 0.334 mol% GdF_3 doped in SrF_2. C_s varied between 0.8 and 11 pF. C_I varied between 2 and 8 pF. ●, data points; ——, theoretical prediction by Eq. (10a). (b) $Q_d d_s$ as a function of C_I/C_s. ●, data points; ——, least-squares fit by Eq. (10b).

B. Dipole peaks

1. Introduction

With ITC experiments, performed on R^{3+}-doped SrF_2, we observed a very characteristic behavior of the dipole concentration as a function of RF_3 concentration. In Fig. 4 we have drawn results obtained for EuF_3-doped SrF_2.[13] The dipole concentration was calculated with Eqs. (4) and (5) where we used $\mu_{NN} = 3.4 \times 10^{-29}$ Cm as obtained in Ref. 22. At low EuF_3 concentrations, the dipole concentration increases linearly with the EuF_3 concentration. At 0.8 mol% EuF_3, a maximum is obtained followed by a slow decrease to zero at 5 mol%. These characteristic features were also observed in CaF_2 crystals doped with RF_3. ITC experiments by Capeletti *et al.*[23] on CaF_2:GdF_3; loss experiments by Campos and Ferreira[24] on CaF_2:CeF_3 and Fontanella and Andeen[25] on CaF_2:ErF_3; laser excitation experiments on CaF_2:ErF_3 by Tallant *et al.*,[26] showed maximum dipole concentrations

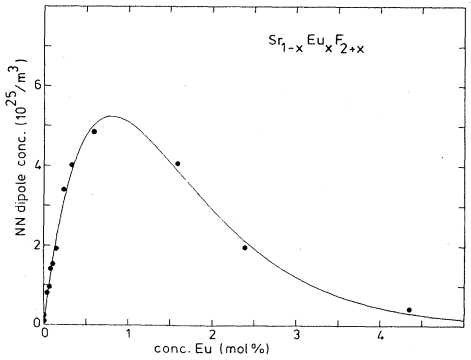

FIG. 4. Concentration of NN dipoles in SrF_2 crystals doped with EuF_3 as a function of EuF_3 concentration. The solid line is obtained by a least-squares fit of Eq. (12).

at about 0.1 mol % rare-earth concentrations. Results obtained for SrF_2 by den Hartog *et al.*[12–16] and Laredo *et al.*[27] revealed maximum dipole intensities varying between 1.5 mol % for SrF_2:LaF_3 and 0.3 mol % for SrF_2:YbF_3.

den Hartog *et al.* proposed the following model to explain the behavior of dipole concentration versus GdF_3 concentration observed with dielectric loss experiments.[14] If two dipoles are close together the reorientation kinetics of $R^{3+}+F^-$ dipoles is likely to be influenced. Therefore, they assume that only isolated dipoles contribute to the dipole relaxation peaks. An isolated dipole is then defined as a dipole not surrounded by a R^{3+} ion within a sphere of radius R, containing N possible R^{3+} sites. The number of possible R^{3+} positions surrounding a central dipole as a function of radius R has been shown in Fig. 5. For large R this can be approximated by the relation

$$N=\tfrac{2}{3}\pi\left[\frac{R}{d_{F^-\text{-}F^-}}\right]^3 \tag{11}$$

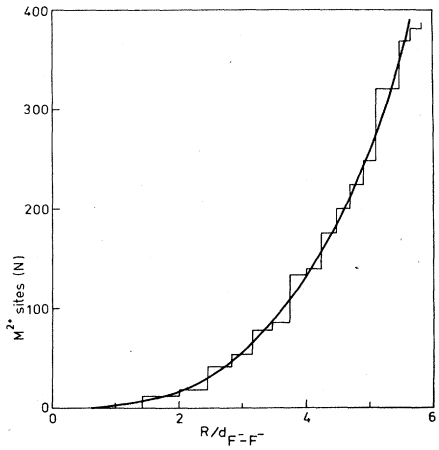

Fig. 5. Number of M^{2+} sites (N) contained in a sphere of radius $R/d_{F^-\text{-}F^-}$ in the MF_2 fluorite lattice. Stepped line, exact number of M^{2+} sites; continuous line, approximate number of M^{2+} sites given by Eq. (11).

where $d_{F^-\text{-}F^-}$ is the F^--F^- distance in the fluorite lattice. ($d_{F^-\text{-}F^-}=2.73$ Å for CaF_2 and 2.90 Å for SrF_2.) If the R^{3+} ions are randomly distributed over the Sr^{2+} lattice sites and a fraction α of the R^{3+} ions form a dipolar complex with an interstitial F^- then the concentration isolated dipoles N_d is given by

$$N_d=\frac{1}{2(d_{F^-\text{-}F^-})^3}\alpha x(1-x)^N \text{ dipoles/m}^3\,, \tag{12}$$

where $1/2(d_{F^-\text{-}F^-})^3$ is the concentration M^{2+} sites in the fluorite lattice and x the fraction M^{2+} ions substituted by a R^{3+} ion. Campos and Ferreira[24] also used the idea of a dipole being isolated in order to explain their results obtained for CaF_2 doped with GdF_3. Using also statistical arguments they arrived at an equation which, for large N and small x, is quite similar to Eq. (12).

2. *Results*

We employed previously published data concerning dipole concentrations in SrF_2 doped with NdF_3, EuF_3, DyF_3, and ErF_3,[12,13,15] and have carried out additional experiments on SrF_2 doped with LaF_3, CeF_3, SmF_3, GdF_3, ErF_3, and LuF_3. The dipole concentrations were calculated with Eqs. (4) and (5). We used for the dipole moment of NN dipoles we value 3.4×10^{-29} C m and for NNN dipoles 8.0×10^{-29} C m. These values were obtained in Ref. 22 for SrF_2 doped with GdF_3. Although some variation of μ as a function of the rare-earth ionic radius might be expected, we used for all R^{3+}-F^- dipoles the same values. A least-squares fit of the calculated dipole concentrations as a function of RF_3 concentration with Eq. (12) provided the parameters α and N. These parameters are compiled in Table I. The errors listed in Table I are standard deviations of the fit parameters α and N and are an indication of the quality of the fit. Due to uncertainties in μ and not taking into account fringing field effects, there might be a systematic error in the parameter α. For instance the high α value for Er-doped SrF_2 ($\alpha=1.35\pm0.11$) might be due to such an error. The best fit is obtained for SrF_2:EuF_3, as shown in Fig. 4, clearly demonstrating the power of Eq. (12). The results in Table I have been visualized in Fig. 6 where we have plotted the fitted relation (12) for some R^{3+} ions in SrF_2. A very clear trend of the behavior of the dipole concentration as a function of rare-earth ionic radius can be observed. Going from La to Lu the ionic radius decreases monotonically[28] as shown in Table I, while the parameter N increases monotonically. Large values of N give rise to an overall decrease of the dipole peak intensity and shift of the maximum dipole concentration towards smaller R^{3+} concentration. Using Eq. (11), N can be converted to $R/d_{F^-\text{-}F^-}$ which has also been compiled in Table I. In Fig. 7, $R/d_{F^-\text{-}F^-}$ is plotted versus the ionic radius of the rare-earth ions; a remarkable linear relationship between R and ionic radius can be observed.

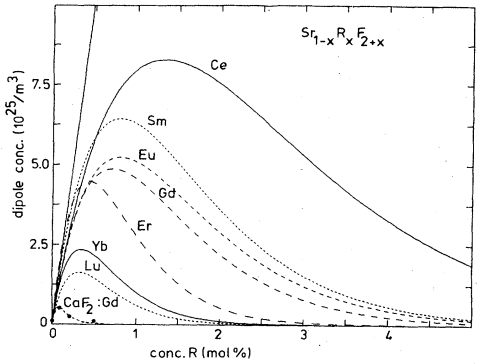

FIG. 6. Concentration of dipoles (NN or NNN) in SrF_2 crystals doped with RF_3 as a function of RF_3 concentration. Equation (12) and the parameters α and N compiled in Table I have been used. R=Ce, Sm, Eu, Gd (NN dipoles), or R=Er, Yb, Lu (NNN dipoles). ●, results obtained by Capelletti *et al.* (Ref. 23) for NN dipoles in GdF_3-doped CaF_2. The straight line represents the concentration of R^{3+} ions.

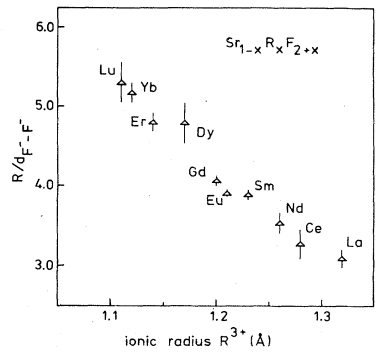

FIG. 7. The value of $R/d_{F^-F^-}$ as a function of rare-earth ionic radius. The results plotted in this figure pertain to solid solutions $Sr_{1-x}R_xF_{2+x}$.

V. DISCUSSION

We shall now discuss the behavior of the parameters α and R, compiled in Table I, as a function of R^{3+} ionic radius. The parameter α is of the order of 1, implying that at low RF_3 concentration in SrF_2, most of the R^{3+} are involved in a dipolar complex. Systematic errors in α are possible because the dipole moment μ is not exactly known.

The parameter R, the minimum distance between isolated dipoles, increases linearly with decreasing ionic radius of the R^{3+}. The minimum R value ($3.1d_{F^-F^-}$ is obtained for LaF_3-doped SrF_2. It is not surprising that La^{3+}-F^- dipoles at smaller distances do not contribute to the NN dipole relaxation peak anymore because at these small separations the dipole almost overlap and the reorientation kinetics is likely to be influenced. Very large R values can be found for CaF_2 doped with RF_3. The maximum dipole intensities occur between 0.05 and 0.1 mol % corresponding with a R value between 8 and 9 $d_{F^-F^-}$. At these distances it is not likely that the reorientation kinetics of a R^{3+}-F^- dipole is drastically influenced. The large difference between dipole concentrations in SrF_2 and CaF_2 is demonstrated by the result obtained by R. Capelletti *et al.*[23] on CaF_2 doped with GdF_3 as shown in Fig. 6. It is now well established that extensive clustering of R^{3+} takes place in CaF_2 crystals.[29–32] An effect of this clustering is the small probability of an isolated dipole to occur resulting in a maximum dipole intensity at low RF_3 concentration. If clustering take place, during growth of the crystals, for two R^{3+} ions located less than 8–9 F^--F^- distances apart then a maximum dipole intensity at 0.05–0.1 mol % will result.

The increase of the parameter R, as the radius of the R^{3+} ion is decreased, can now be understood if an increasing clustering probability is assumed when going from La to Lu. In SrF_2 doped with LaF_3 clustering of La^{3+} ions is then rather unimportant, expressed by the

TABLE I. Values of α and N [obtained by Eq. (12) and converted to $R/d_{F^-F^-}$ by Eq. (11)] as a function of ionic radius of the R^{3+} ion for different kinds of dipole types in SrF_2.

R^{3+}	α	N	Dipole type	Ionic radius (Å)	$\frac{R}{d_{F^-F^-}}$
La	0.66±0.15	62± 7	NN	1.32	3.09±0.11
Ce	0.81±0.14	74±13	NN	1.28	3.28±0.20
Nd	1.10±0.13	92± 9	NN	1.26	3.53±0.11
Sm	1.04±0.06	123± 6	NN	1.23	3.89±0.06
Eu	0.86±0.05	124± 4	NN	1.21	3.90±0.05
Gd	0.90±0.04	140± 5	NN	1.20	4.06±0.05
Gd	0.11±0.02	115±20	NNN	1.20	3.80±0.21
Dy	0.87±0.18	230±40	NNN	1.17	4.79±0.27
Er	1.35±0.11	231±13	NNN	1.14	4.80±0.10
Yb	0.89±0.08	290±18	NNN	1.12	5.17±0.11
Lu	0.67±0.14	310±50	NNN	1.11	5.29±0.25

small R value, while in SrF_2 doped with LuF_3 clustering takes place, though not as extensive as in CaF_2 doped with RF_3. This assumption is strongly supported by Andeen *et al.*[14] who performed dielectric relaxation experiments on CaF_2, SrF_2, and BaF_2 doped with 0.1 mol% and 1 mol% RF_3. They concluded that the number and intensity of cluster associated relaxation peaks in the dielectric spectrum increases as both the size of the host (Ba—Sr—Ca) and rare earth (La—Lu) decreases. In general there is also more clustering with increasing RF_3 concentrations. In CaF_2 extensive clustering takes place and in SrF_2 doped with RF_3 probability for clustering increases in going from large R^{3+} ions (La,Ce) toward small ions (Yb,Lu). The increases of the concentrations of clusters and the corresponding decrease of isolated dipoles as a function of RF_3 concentration is already expressed by Eq. (12).

EPR experiments performed by Brown *et al.*[33] on SrF_2 doped with CeF_3 and ErF_3 are in agreement with our ITC results. To explain the observed decrease of trigonal sites (NNN dipoles) for ErF_3 concentrations in SrF_2 higher than 0.3 mol%, they assumed association of Er^{3+} ions with dislocations present in the crystal. We believe that association of Er^{3+} with other Er^{3+} (clustering) can be held equally well responsible. This is supported by laser excitation experiments performed on ErF_3 doped SrF_2 by Kurz and Wright.[34] These authors observed Er^{3+} sites associated with complex clusters.

The different behavior of rare-earth ions from opposite ends of the lanthanide series when doped in SrF_2 also has consequences for the space-charge conduction peak observed with ITC. LaF_3-,[10] CeF_3-,[11] PrF_3-, and NdF_3-(Ref. 12) doped SrF_2 show a large monotonic decrease of peak position towards lower temperatures as the RF_3 concentration is increased, while ErF_3,[15] YbF_3,[16] and LuF_3 in SrF_2 show an oscillating behavior. Intermediate between these characteristic behaviors are EuF_3,[13] SmF_3, GaF_3, and DyF_3-(Ref. 15) doped SrF_2; the elements from the central part of the lanthanide series. The plots of peak positions (T_{max}) versus concentration, for the above mentioned RF_3-doped SrF_2 crystals, can be seen in Fig. 8. Most of these plots have been published before[10–13,15,16] (La, Ce, Nd, Eu, Dy, Er, and Yb), Pr, Sm, Gd, and Lu are presented for the first time. The position of the HT peak is related with the conductivity of the sample material as expressed by Eq. (8). In order to explain the conductivity of the crystals, den Hartog *et al.* assumed clustering to be present for Dy-, Er-, Yb-, and Lu-doped SrF_2, while it is of minor importance for La-, Ce-, Pr-, and Nd-doped SrF_2. This assumption is now supported by the results obtained for the dipole concentrations.

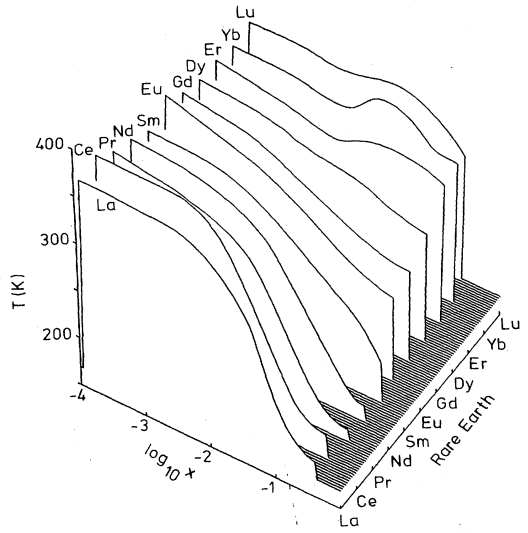

FIG. 8. Three-dimensional plot of the position of the HT peak as a function of RF_3 concentration doped in SrF_2 as observed with ITC experiments. 0.1-mm Teflon foils have been used as insulating material. The heating rate was 0.05 K/s except for R=La, Nd, and Yb, where a heating rate of 0.03 K/s was used. The data points have been left out; they usually do not deviate more than 5 K from the drawn curves.

VI. CONCLUSIONS

ITC experiments performed on RF_3-doped SrF_2 as a function of rare-earth radius and concentration leads us to the following conclusions.

(i) The high-temperature peak is clearly connected with space-charge relaxation. The intensity and the shift of the maximum position with sample and insulation thickness can be completely accounted for.

(ii) The characteristic behavior of the dipole concentration as a function of RF_3 concentration can be understood by a simple statistical model expressed by Eq. (12).

(iii) The decrease of the dipole intensity and the shift of the maximum dipole concentration towards lower R^{3+} concentrations in RF_3-doped SrF_2, as the ionic radius of R^{3+} decreases, is probably due to increasing clustering probability of the R^{3+} ions.

(iv) For LaF_3, CeF_3, PrF_3, and NdF_3 doped in SrF_2, clustering is rather unimportant.

[1]D. R. Stiefbold and R. A. Huggins, J. Solid State Chem. **5**, 15 (1972).

[2]E. L. Kitts and J. H. Crawford, Phys. Rev. B **9**, 9 (1974).

[3]C. Andeen, D. Link, and J. Fontanella, Phys. Rev. B **16**, 3762 (1977).

[4]C. G. Andeen, J. J. Fontanella, M. C. Wintersgill, P. J. Welcher, R. J. Kimble, and G. E. Matthews, J. Phys. C **14**, 3557 (1981).

[5]B. P. M. Lenting, J. A. J. Numan, E. J. Bijvank, and H. W. den Hartog, Phys. Rev. B **14**, 1811 (1976).

[6]E. Laredo, D. R. Figueroa, and M. Puma, J. Phys. (Paris) C **6**, C6-451 (1980).

[7]I. V. Murin, A. V. Glumov, and V. M. Reiterov, Fiz. Tverd. Tela (Leningrad) **21**, 298 (1979) [Sov. Phys. Solid State **21**, 180 (1979).
[8]I. Kunze and P. Müller, Phys. Status Solidi A **13**, 197 (1972).
[9]N. Kristianpoller and Y. Kirsh, Phys. Status Solidi A **21**, 87 (1974).
[10]J. Meuldijk and H. W. den Hartog, Phys. Rev. B **28**, 1036 (1983).
[11]J. Meuldijk, R. van der Meulen, and H. W. den Hartog, Phys. Rev. B **29**, 2153 (1984).
[12]J. Meuldijk, H. H. Mulder, and H. W. den Hartog, Phys. Rev. B **25**, 5204 (1982).
[13]H. W. den Hartog and R. Nakata, J. Phys. Soc. Jpn. **52**, 3110 (1983).
[14]H. W. den Hartog and J. Meuldijk, Phys. Rev. B **29**, 2210 (1984).
[15]J. Meuldijk, G. Kiers, and H. W. den Hartog, Phys. Rev. B **28**, 6022 (1983).
[16]J. Meuldijk and H. W. den Hartog, Phys. Rev. B **27**, 6376 (1983).
[17]R. J. Kimble, P. J. Welcher, J. J. Fontanella, M. C. Wintersgill, and C. G. Andeen, J. Phys. C **15**, 3441 (1982).
[18]J. Corish, C. R. A. Catlow, P. W. M. Jacobs, and S. H. Ong, Phys. Rev. B **25**, 6425 (1982).
[19]P. Müller, Phys. Status Solidi A **67**, 11 (1981).
[20]J. R. MacDonald, J. Chem. Phys. **29**, 1346 (1958).
[21]J. R. MacDonald, J. Chem. Phys. **30**, 806 (1959).
[22]A. B. Aalbers and H. W. den Hartog, Phys. Rev. B **19**, 2163 (1979).
[23]R. Capelletti, E. Okuno, G. E. Matthews, and J. H. Crawford, Phys. Status Solidi A **47**, 617 (1978).
[24]V. B. Campos and G. F. L. Ferreira, J. Phys. Chem. Solids **35**, 905 (1974).
[25]J. Fontanella and C. Andeen, J. Phys. C **9**, 1055 (1976).
[26]D. R. Tallant, D. S. Moore, and J. C. Wright, J. Chem. Phys. **67**, 2897 (1977).
[27]E. Laredo, M. Puma, N. Suarez, and D. R. Figueroa, Phys. Rev. B **23**, 3009 (1981).
[28]R. D. Shannon and C. T. Prewitt, Acta Crystallogr. Sect. B **25**, 925 (1969).
[29]R. J. Booth and B. R. McGarvey, Phys. Rev. B **21**, 1627 (1980).
[30]M. B. Seelbinder and J. C. Wright, Phys. Rev. B **20**, 4308 (1979).
[31]R. H. Petit, P. Evesque, and J. Duran, J. Phys. C **14**, 5081 (1981).
[32]R. J. Booth, M. R. Mustafa, and B. R. McGarvey, Phys. Rev. B **17**, 4150 (1978).
[33]M. R. Brown, H. Thomas, J. S. S. Whiting, and W. A. Shand, J. Chem. Phys. **50**, 881 (1969).
[34]M. D. Kurz and J. C. Wright, J. Lumin. **15**, 169 (1977).